Science Signaling
AAAS
www.sciencesignaling.org/cgi/content/full/5/226/ra39/DC1

Supplementary Materials for

Sequence-Specific Recognition of a PxLPxI/L Motif by an Ankyrin Repeat Tumbler Lock

Chao Xu, Jing Jin, Chuanbing Bian, Robert Lam, Ruijun Tian, Ryan Weist, Linya You, Jianyun Nie, Alexey Bochkarev, Wolfram Tempel, Chris S. Tan, Gregory A. Wasney, Masoud Vedadi, Gerald D. Gish, Cheryl H. Arrowsmith, Tony Pawson, Xiang-Jiao Yang, Jinrong Min*

*To whom correspondence should be addressed. E-mail: jr.min@utoronto.ca

Published 29 May 2012, *Sci. Signal.* **5**, ra39 (2012)
DOI: 10.1126/scisignal.2002979

The PDF file includes:

Materials and Methods
Fig. S1. Sequence of the peptides on the spot array.
Fig. S2. Crystal structures of apo-ANKRA2 and its complexes with the megalin peptides.
Fig. S3. Sequence alignment and structural comparison of ANKRA2 and RFXANK.
Fig. S4. Arg^{199} of RFXANK is critical to determining its ligand-binding specificity.
Fig. S5. Detailed electrospray ionization (ESI)–MS/MS spectrum analysis of $pSer^{350}$ of HDAC4.
Fig. S6. Resemblance among repeat-type domains with respect to their ligand-binding modes.
Table S1. Data collection and refinement statistics.
References

Materials and Methods

Crystallization of ANKRA2, RFXANK, and their complexes

The apo form of the ANKRA2 ankyrin repeat (residues 142 to 313) was crystallized in a buffer containing 0.2 M sodium acetate and 25% PEG3350. ANKRA2 (residues 148 to 313) and the shorter megalin peptide (residues 4455 to 4465) were mixed in a molar ratio of 1:3 and crystallized in a buffer containing 0.1 M bis-tris HCl (pH 6.5), 0.2 M NaCl, and 25% PEG3350. 6 × His-tagged ANKRA2 (residues 148 to 313) and the longer megalin peptide (residues 4448 to 4466) were mixed in a molar ratio of 1:2 and crystallized in a buffer containing 0.1 M hepes (pH 7.5), 0.2 M ammonium acetate, and 25% PEG3350. ANKRA2 (residues 148 to 313) and the HDAC4 peptide (residues 343 to 359) were mixed in a ratio of 1:2 and crystallized in a buffer containing 0.1 M bis-tris HCl (pH 6.5), 0.2 M NaCl, and 25% PEG3350. RFXANK (residues 90 to 260) and the RFX5 peptide (residues 167 to 183) were mixed in a ratio of 1:5 and crystallized in a buffer containing 0.1 M bis-tris HCl (pH 6.5), 0.2 M ammonium acetate, and 25% PEG 3350. RFXANK-R199H (residues 90 to 260) and the HDAC4 peptide (residues 343 to 359) were mixed in a ratio of 1:3 and crystallized in a buffer containing: 0.1 M hepes (pH 7.5), 0.2 M NaCl, and 25% PEG3350. 14-3-3γ was purified as described previously (*1*) and concentrated to 30 mg/ml in a buffer containing 20 mM tris-HCl (pH 7.5), 150 mM NaCl, 1 mM dithiothreitol (DTT). 14-3-3γ was then mixed with the $pSer^{350}$ HDAC4 peptide (residues 343 to 359) in a ratio of 3:1 and crystallized in a buffer containing 0.3 M magnesium acetate and 20% PEG3350. Before flash-freezing in liquid nitrogen, all of the crystals were soaked in a cryoprotectant consisting of 85 to 90% reservoir solution and 10 to 15% glycerol (v/v).

Data collection, structure determination, and refinement

Diffraction data were collected at 100K either on a beamline 19-ID (Structural Biology Centre, Advanced Photon Source, Argonne National Laboratory) or using CuKα radiation generated on a Rigaku FR-E SuperBright rotating anode system equipped with a Saturn A200 CCD detector. Datasets were integrated and scaled with the HKL2000 software package (*2*), with the exception of the RFXANK(R199H)-HDAC4 complex, for which XDS (*3*), POINTLESS (*4*) and SCALA (*5*) were used. The Apo-ANKRA structure was determined by standard SeMet method. All peptide-bound ankyrin repeat structures were solved by molecular replacement method using either the MOLREP (*6*) or PHASER (*7*) module in the CCP4 program suite (http://www.ccp4.ac.uk) using the apo-structure as a search model. After several alternate cycles of manual rebuilding with COOT (*8*) and restrained refinement against a maximum likelihood target, the improved models revealed clear electron densities that enabled placement of the bound peptides as well as of the ordered solvent molecules. All refinement steps were performed with REFMAC (*9*) in the CCP4 program suite. Translation-libration-screw (TLS) parameterization (*10*) was included in the final refinement of all models. Model geometry was validated on the MOLPROBITY server (*11*). Restraints for bis-tris geometry were generated by the PRODRG server (*12*). Data collection and refinement statistics are summarized in table S1.

MS analysis

Protein samples from immunoprecipitations were loaded onto a strong cation exchange (SCX) resin and then digested by trypsin and chymotrypsin in tandem. The obtained peptides were further enriched for phosphopeptides by MonoTip TiO_2 (GL Sciences) according to the manufacturer's standard protocols. After elution, the phosphopeptides were dried and then prepared in 0.1% (v/v) formic acid for mS analysis. Samples were analyzed by a nano LC-MS/MS system that consisted of a frontline Eksigent nano LC (model Ultra1D) and an LTQ-Orbitrap mass spectrometer (Thermo). The flow rate on nano LC was

controlled at 400 nl/min for sample loading and 200 nl/min for analysis. The 30- or 90-min gradients were formed as 5 to 35% (v/v) of ACN/0.1% formic acid (v/v). The peptides were separated by a tip column (75 μm ID × 10 cm) packed with 3 μm/120 Å ReproSil-Pur C18 resins (Dr. Maisch GmbH, Ammerbuch, Germany). The spray voltage was set at +1.8 kV, and collision energy was set at 35%. The mass spectrometer was operated in a data-dependent mode with one MS scan followed by three MS/MS scans. The MS scans were acquired at a resolution of 60,000. The obtained raw files were converted to mgf files by the in-house software Prohits (The Samuel Lunenfeld Research Institute, ON, Canada). The Human NCBI Reference Sequence database (version 29, 38063 sequences) was searched by mascot (version 2.0.0.0, Matrix Science) with the following parameters: mass tolerance: 7 ppm on MS and 0.5 Daltons on MS/MS; maximum missed cleavages: 2; fixed modification: carbamidomethyl (C); variable modification: oxidation (M), phospho (ST) and phospho (Y).

	a (1-113)	b (101-213)	c(201-313)	d (301-413)	e (401-513)	f (501-613)	g (601-708)
1	MSSQSHPDGLSGRDQPVE	SRQHEAQLHEHIKQQQEM	YWYGKTQHSSLDQSSPPQ	SSPNNSSGSVSAENGIAP	PLERDGGAAHSPLLQHMV	QLQMNKIIPKPSEPARQP	RIHQLRNYQASMEAAGIP
2	HPDGLSGRDQPVELLNPA	AQLHEHIKQQQEMLAMKH	TQHSSLDQSSPPQSGVST	SSGSVSAENGIAPAVPSI	GGAAHSPLLQHMVLLEQP	KIIPKPSEPARQPESHPE	RNYQASMEAAGIPVSFGG
3	SGRDQPVELLNPARVNHM	HIKQQQEMLAMKHQQELL	LDQSSPPQSGVSTSYNHP	SAENGIAPAVPSIPAETS	SPLLQHMVLLEQPPAQAP	PSEPARQPESHPEETEEE	SMEAAGIPVSFGGHRPLS
4	PVELLNPARVNHMPSTVD	QEMLAMKHQQELLEHQRK	PPQSGVSTSYNHPVLGMY	IAPAVPSIPAETSLAHRL	HMVLLEQPPAQAPLVTGL	RQPESHPEETEEELREHQ	GIPVSFGGHRPLSRAQSS
5	NPARVNHMPSTVDVATAL	MKHQQELLEHQRKLERHR	VSTSYNHPVLGMYDAKDD	PSIPAETSLAHRLVAREG	EQPPAQAPLVTGLGALPL	HPEETEEELREHQALLDE	FGGHRPLSRAQSSPASAT
6	NHMPSTVDVATALPLQVA	ELLEHQRKLERHRQEQEL	NHPVLGMYDAKDDFPLRK	ETSLAHRLVAREGSAAPL	QAPLVTGLGALPLHAQSL	EEELREHQALLDEPYLDR	PLSRAQSSPASATFPVSV
7	TVDVATALPLQVAPSAVP	QRKLERHRQEQELEKQHR	GMYDAKDDFPLRKTASEP	HRLVAREGSAAPLPLYTS	TGLGALPLHAQSLVGADR	EHQALLDEPYLDRLPGQK	QSSPASATFPVSVQEPPT
8	TALPLQVAPSAVPMDLRL	RHRQEQELEKQHREQKLQ	KDDFPLRKTASEPNLKLR	REGSAAPLPLYTSPSLPN	LPLHAQSLVGADRVSPSI	LDEPYLDRLPGQKEAHAQ	SATFPVSVQEPPTKPRFT
9	QVAPSAVPMDLRLDHQFS	QELEKQHREQKLQQLKNK	LRKTASEPNLKLRSRLKQ	APLPLYTSPSLPNITLGL	QSLVGADRVSPSIHKLRQ	LDRLPGQKEAHAQAGVQV	VSVQEPPTKPRFTTGLVY
10	AVPMDLRLDHQFSLPVAE	QHREQKLQQLKNKEKGKE	SEPNLKLRSRLKQKVAER	YTSPSLPNITLGLPATGP	ADRVSPSIHKLRQHRPLG	GQKEAHAQAGVQVKQEPI	PPTKPRFTTGLVYDTLML
11	LRLDHQFSLPVAEPALRE	KLQQLKNKEKGKESAVAS	KLRSRLKQKVAERRSSPL	LPNITLGLPATGPSAGTA	PSIHKLRQHRPLGRTQSA	HAQAGVQVKQEPIESDEE	RFTTGLVYDTLMLKHQCT
12	QFSLPVAEPALREQQLQQ	KNKEKGKESAVASTEVKM	LKQKVAERRSSPLLRRKD	LGLPATGPSAGTAGQQDA	LRQHRPLGRTQSAPLPQN	VQVKQEPIESDEEEAEPP	LVYDTLMLKHQCTCGSSS
13	VAEPALREQQLQQELLAL	GKESAVASTEVKMKLQEF	AERRSSPLLRRKDGPVVT	TGPSAGTAGQQDAERLTL	PLGRTQSAPLPQNAQALQ	EPIESDEEEAEPPREVEP	LMLKHQCTCGSSSSHPEH
14	LREQQLQQELLALKQKQQ	VASTEVKMKLQEFVLNKK	SPLLRRKDGPVVTALKKR	GTAGQQDAERLTLPALQQ	QSAPLPQNAQALQHLVIQ	DEEEAEPPREVEPGQRQP	QCTCGSSSSHPEHAGRIQ
15	LQQELLALKQKQQIQRQI	VKMKLQEFVLNKKKALAH	RKDGPVVTALKKRPLDVT	QDAERLTLPALQQRLSLF	PQNAQALQHLVIQQQHQQ	EPPREVEPGQRQPSEQEL	SSSSHPEHAGRIQSIWSR
16	LALKQKQQIQRQILIAEF	QEFVLNKKKALAHRNLNH	VVTALKKRPLDVTDSACS	LTLPALQQRLSLFPGTHL	ALQHLVIQQQHQQFLEKH	VEPGQRQPSEQELLFRQQ	PEHAGRIQSIWSRLQETG
17	KQQIQRQILIAEFQRQHE	NKKKALAHRNLNHCISSD	KKRPLDVTDSACSSAPGS	LQQRLSLFPGTHLTPYLS	VIQQQHQQFLEKHKQQFQ	RQPSEQELLFRQQALLLE	RIQSIWSRLQETGLRGKC
18	RQILIAEFQRQHEQLSRQ	LAHRNLNHCISSDPRYWY	DVTDSACSSAPGSGPSSP	SLFPGTHLTPYLSTSPLE	HQQFLEKHKQQFQQQQLQ	QELLFRQQALLLEQQRIH	WSRLQETGLRGKCECIRG
19	AEFQRQHEQLSRQHEAQL	LNHCISSDPRYWYGKTQH	ACSSAPGSGPSSPNNSSG	THLTPYLSTSPLERDGGA	EKHKQQFQQQQLQMNKII	RQQALLLEQQRIHQLRNY	ETGLRGKCECIRGRKATL
20	QHEQLSRQHEAQLHEHIK	SSDPRYWYGKTQHSSLDQ	PGSGPSSPNNSSGSVSAE	YLSTSPLERDGGAAHSPL	QFQQQQLQMNKIIPKPSE	LLEQQRIHQLRNYQASME	HHHHHH

Fig. S1. Sequence of the peptides on the spot array. The ANKRA2-binding sequence of HDAC4 and the positive control sequence are marked in red and blue, respectively.

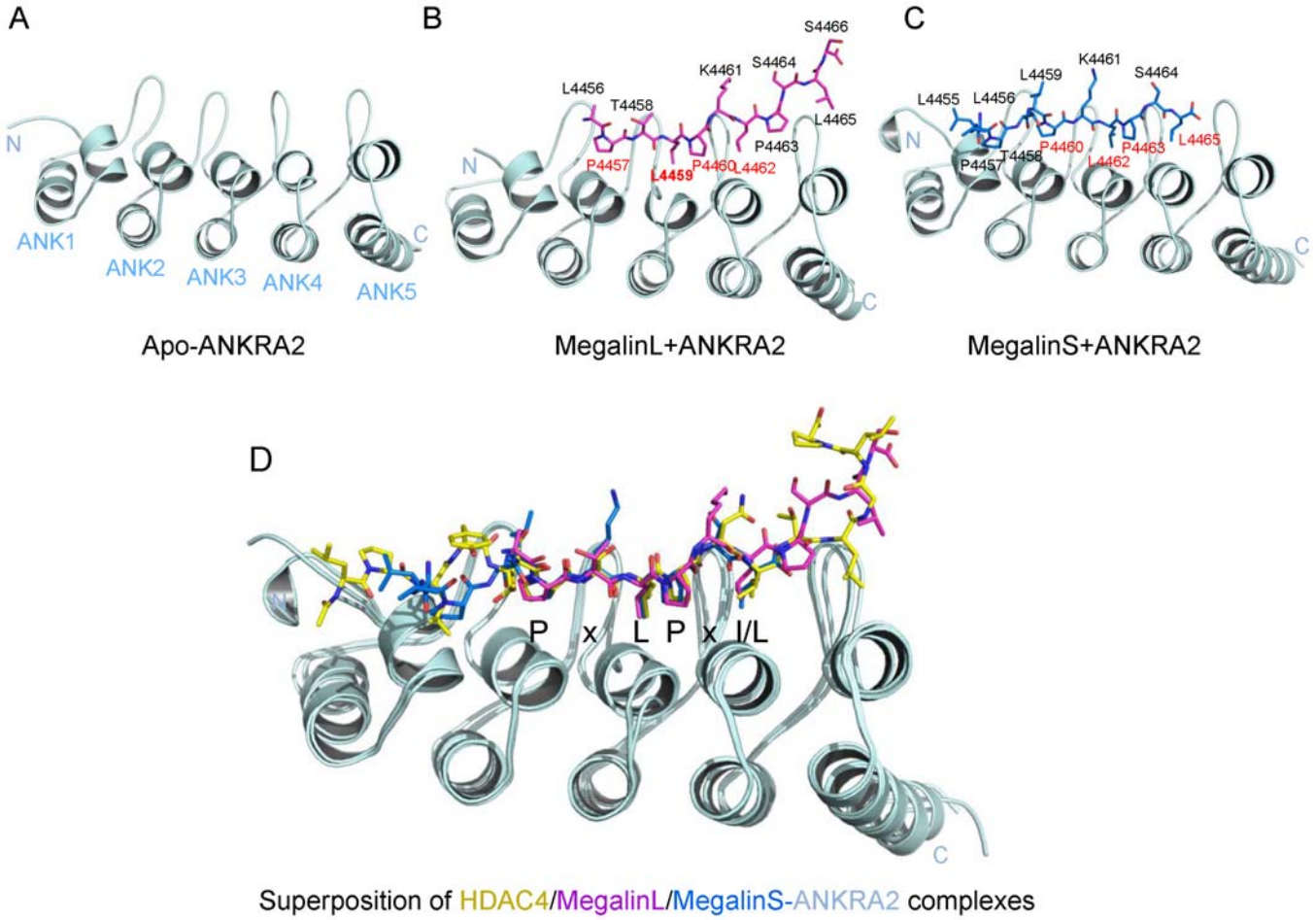

Fig. S2. Crystal structures of apo-ANKRA2 and its complexes with the megalin peptides. (**A**) Crystal structure of the free ankyrin repeat domain of ANKRA2, which consists of five ankyrin repeats, including two capping repeats and three middle repeats (ANK1 to ANK5). (**B**) Crystal structure of ANKRA2 in complex with the long megalin peptide (residues 4448 to 4466). The protein is shown as a pale cyan cartoon, whereas the peptide is shown as magenta sticks. (**C**) Crystal structure of ANKRA2 in complex with the short megalin peptide (residues 4455 to 4465). The protein is shown as a pale cyan cartoon, whereas the peptide is shown as blue sticks. (**D**) Superposition of the ANKRA2 structures in complex with the HDAC4 (yellow), MegalinL (magenta), and MegalinS (blue) peptides. The peptides are shown as colored sticks and ANKRA2 is shown as a pale cyan cartoon. The three peptides share a similar conformation in the complex structures and the PxLPxI/L consensus motif is marked.

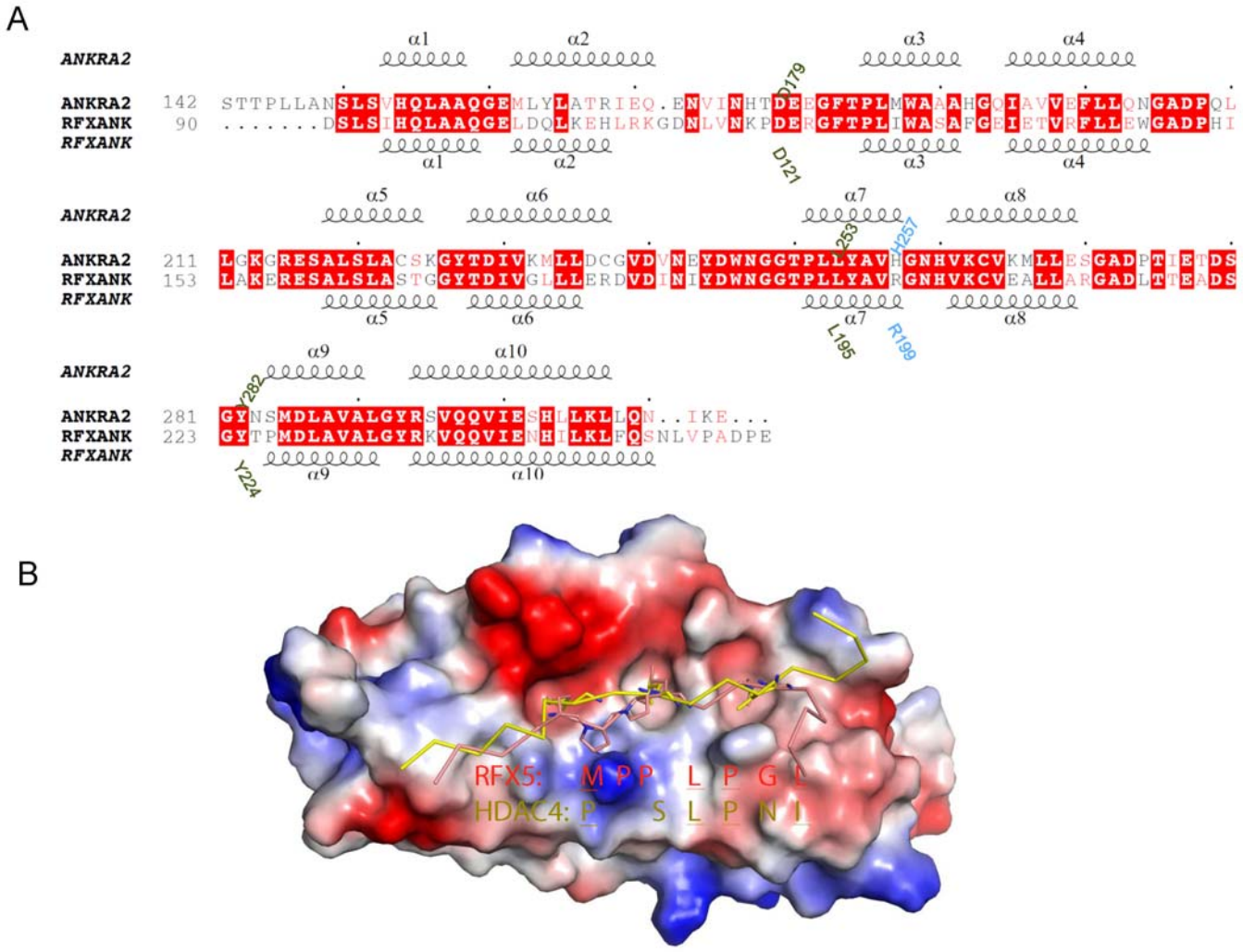

Fig. S3. Sequence alignment and structural comparison of ANKRA2 and RFXANK. (**A**) Sequence alignment of ANKRA2 and RFXANK. Some critical residues of ANKRA2 and RFXANK mentioned in the text are marked. (**B**) Superposition of the ANKRA2-HDAC4 and RFXANK-RFX5 complexes. ANKRA2 is shown as a surface representation, and HDAC4 and RFX5 are shown as ribbons and are labeled in yellow and red, respectively.

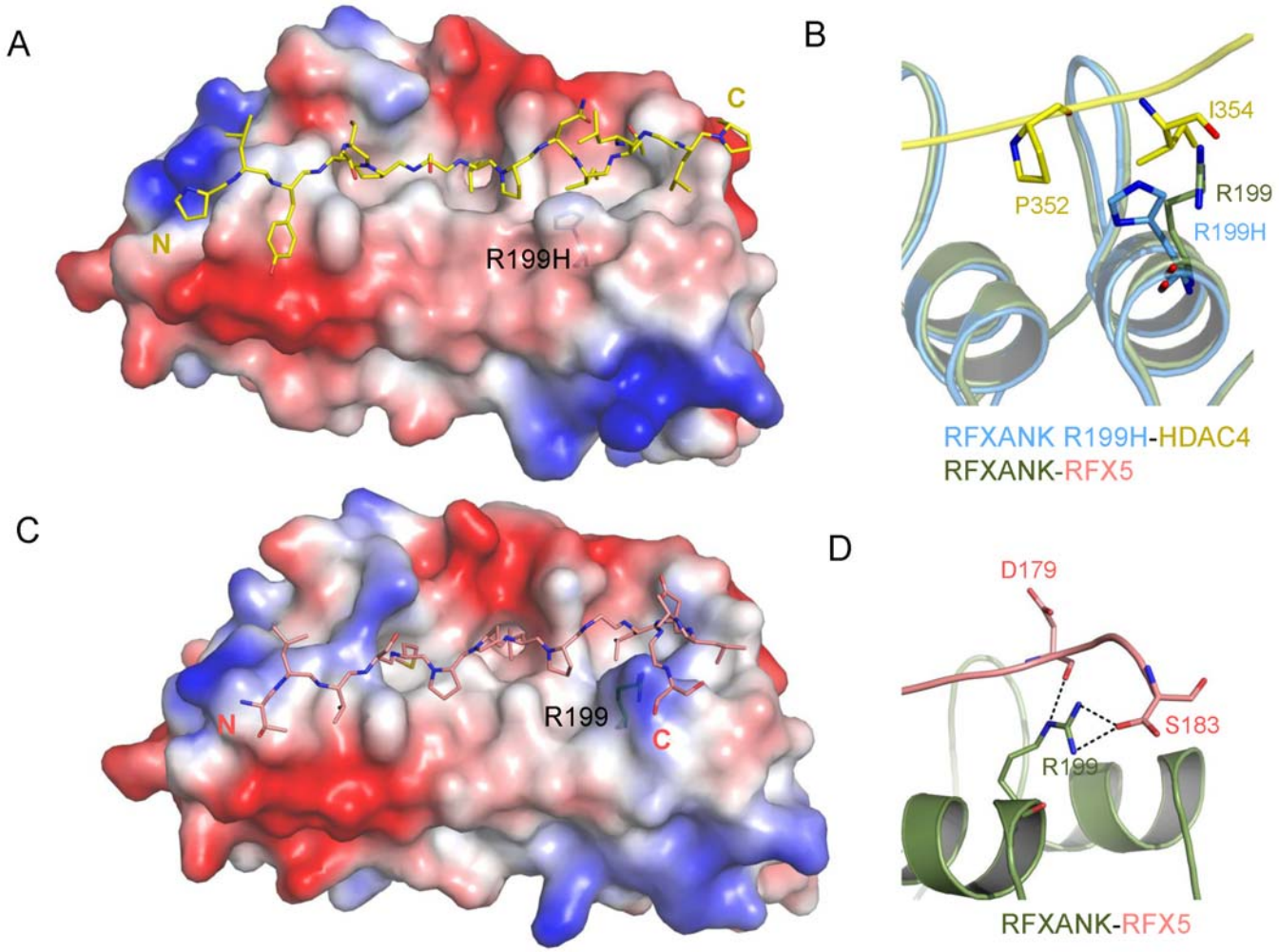

Fig. S4. Arg[199] of RFXANK is critical to determining its ligand-binding specificity. (**A**) Structure of the complex of mutant R199H RFXANK and HDAC4. The mutant RFXANK is shown as a surface representation with R199H shown as a stick model. The HDAC4 peptide is shown as a yellow stick model. (**B**) Superposition of the structures of the mutant R199H RFXANK-HDAC4 complex and the RFXANK-RFX5 complex, which shows that R199H interacts extensively with P352 and I354 of HDAC4. The mentioned residues are shown as colored sticks. (**C**) Structure of the RFXANK-HDAC4 complex. RFXANK is shown as a surface representation with R199 shown as a stick model. The RXF5 peptide is shown as a yellow stick model. (**D**) In the RFXANK-RFX5 structure, Arg[199] forms three hydrogen bonds with Asp[179] (D179) and Ser[183] (S183) of RFX5.

A

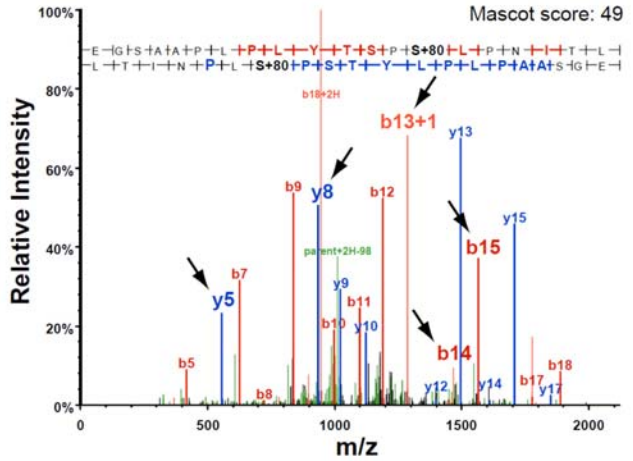

B	B Ions	B+2H	B-NH3	B-H2O	AA	Y Ions	Y+2H	Y-NH3	Y-H2O	Y
1	130.1			112.0	E	2,121.1		2,104.0	2,103.0	20
2	187.1			169.1	G	1,992.0		1,975.0	1,974.0	19
3	274.1			256.1	S	1,935.0		1,918.0	1,917.0	18
4	345.1			327.1	A	1,848.0		1,830.9	1,829.9	17
5	416.2			398.2	A	1,776.9		1,759.9	1,758.9	16
6	513.2	257.1		495.2	P	1,705.9		1,688.9	1,687.9	15
7	626.3	313.7		608.3	L	1,608.8		1,591.8	1,590.8	14
8	723.4	362.2		705.4	P	1,495.7		1,478.7	1,477.7	13
9	836.5	418.7		818.4	L	1,398.7		1,381.7	1,380.7	12
10	999.5	500.3		981.5	Y	1,285.6		1,268.6	1,267.6	11
11	1,100.6	550.8		1,082.6	T	1,122.5		1,105.5	1,104.5	10
12	1,187.6	594.3		1,169.6	S	1,021.5		1,004.5	1,003.5	9
13	1,284.6	642.8		1,266.6	P	934.5		917.4	916.5	8
14	1,451.6	726.3		1,433.6	S+80	837.4		820.4	819.4	7
15	1,564.7	782.9		1,546.7	L	670.4		653.4	652.4	6
16	1,661.8	831.4		1,643.8	P	557.3		540.3	539.3	5
17	1,775.8	888.4	1,758.8	1,757.8	N	460.3		443.3	442.3	4
18	1,888.9	945.0	1,871.9	1,870.9	I	346.2			328.2	3
19	1,990.0	995.5	1,972.9	1,971.9	T	233.2			215.1	2
20	2,121.1	1,061.0	2,104.0	2,103.0	L	132.1				1

B

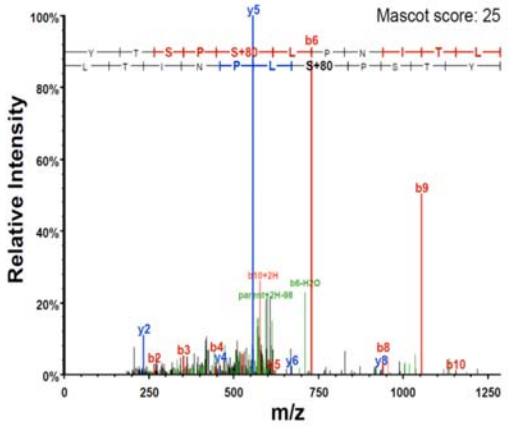

B	B Ions	B+2H	B-NH3	B-H2O	AA	Y Ions	Y+2H	Y-NH3	Y-H2O	Y
1	164.1				Y	1,285.6		1,268.6	1,267.6	11
2	265.1			247.1	T	1,122.5		1,105.5	1,104.5	10
3	352.2			334.1	S	1,021.5		1,004.5	1,003.5	9
4	449.2			431.2	P	934.5		917.4	916.5	8
5	616.2			598.2	S+80	837.4		820.4	819.4	7
6	729.3	365.1		711.3	L	670.4		653.4	652.4	6
7	826.3	413.7		808.3	P	557.3		540.3	539.3	5
8	940.4	470.7	923.4	922.4	N	460.3		443.3	442.3	4
9	1,053.5	527.2	1,036.4	1,035.5	I	346.2			328.2	3
10	1,154.5	577.8	1,137.5	1,136.5	T	233.2			215.1	2
11	1,285.6	643.3	1,268.6	1,267.6	L	132.1				1

Fig. S5. Detailed ESI-MS/MS spectrum analysis of pSer^{350} of HDAC4. (**A**) Analysis of the chymotryptic phospho-peptide EGSAAPLPLYTSP<u>S</u>^{350}LPNITL (also shown in Fig. 3A). Top: spectrum map. The prominent *b*-series ions *b*13, 14, 15 and *y*-series ions *y*5 and *y*8 (pointed by arrows) present unambiguous evidence for pSer^{350} (marked as S+80). Bottom: Theoretical M/Z values of *b*- and *y*-ions on the basis of a presumed pSer^{350}. Spectrum-matched *b*- and *y*-ions are highlighted with red and blue backgrounds, respectively. (**B**) A second phospho-peptide YTSP<u>S</u>^{350}LPNITL presented as additional evidence for the phosphorylation of Ser^{350}**.** Similar to (A), both the *y*- and *b*-series of ions indicate that the peptide is phosphorylated on Ser^{350}.

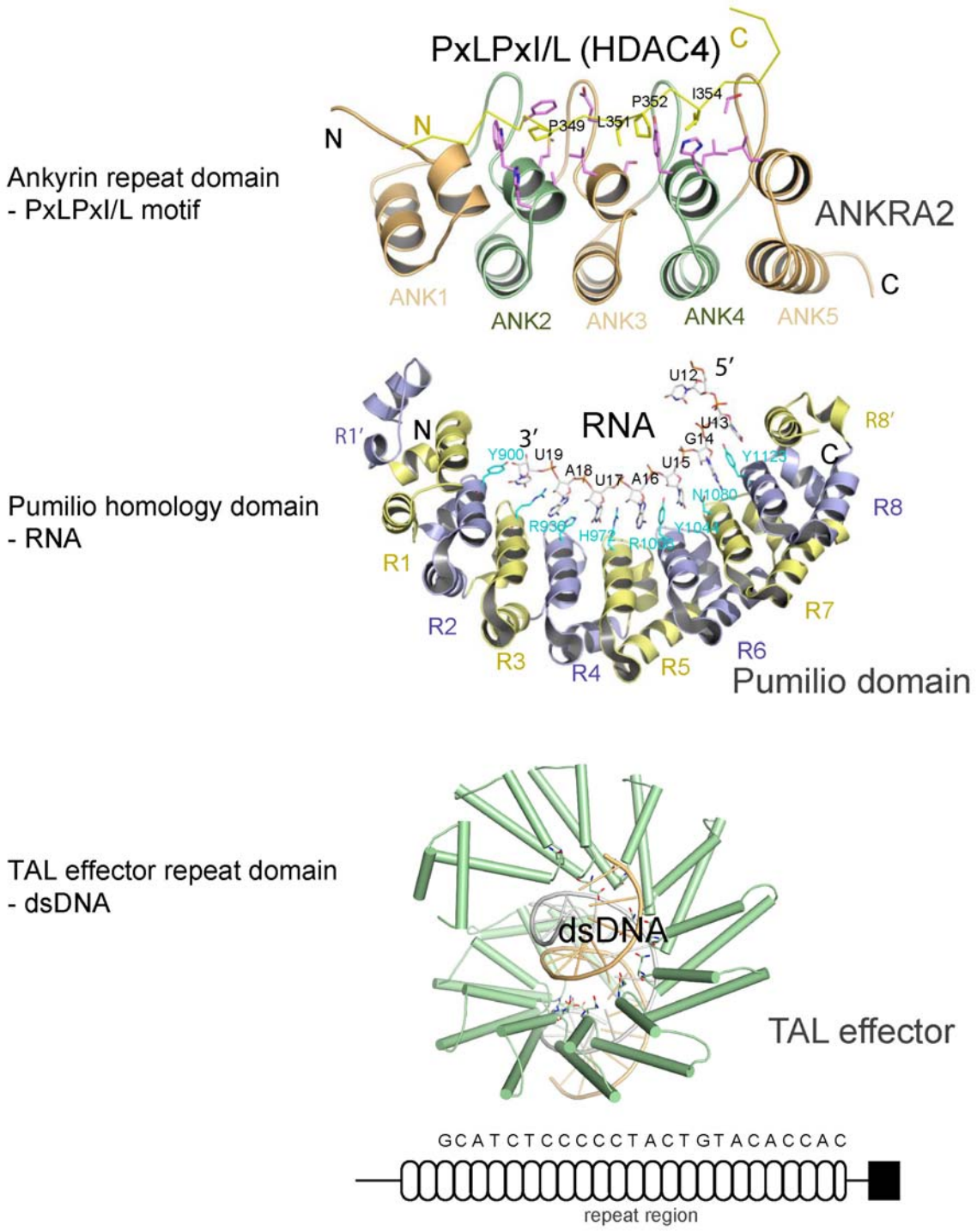

Figure S6. Resemblance among repeat-type domains with respect to their ligand-binding modes. The ankyrin repeat domain, Pumilio homology domain, and the TAL effector domain are compared in terms of the sequence-specific recognition of their peptide, RNA, or DNA binding partners, respectively. Presentation of the TAL effector binding mode was adapted from Mak *et al*. and Deng *et al*. (*13*, *14*).

Table S1. Data collection and refinement statistics.

Crystal structures	Apo-ANKRA2	ANKRA2 + HDAC4 (LPLYTSPSLPNITLGLP)	ANKRA2 + Megalin (HYRKTGSLLPTLPKLPSLS)	ANKRA2+Megalin (LLPTLPKLPSL)	14-3-3 γ+ HDAC4 pSer^{350} (LPLYTSPSLPNITLGLP)	RFXANK + RFX5 (KTLVSMPPLPGLDLKGS)	RFXANK + HDAC4 (LPLYTSPSLPNITLGLP)
Data collection							
Space group	$P2_1$	$P2_1$	$P2_1$	P1	I222	C2	$C222_1$
Cell dimensions							
a, *b*, *c* (Å)	39.1, 40.8, 99.1	29.7, 52.8, 51.6	38.3, 49.6, 41.1	30.0, 32.8, 45.3	60.5, 79.2, 122.2	108.8, 31.5, 63.1	43.6, 98.4, 99.4
α, β, γ (º)	90, 90, 90	90, 98.0, 90	90, 97.5, 90	78.5, 75.2, 66.0	90, 90, 90	90, 107.5, 90	90, 90, 90
Wavelength (Å)	1.54178	0.97931	0.97941	1.54178	0.97941	0.97924	0.97911
Resolution (Å)	50.0-1.90 (1.90-1.95)*	50.0-1.57 (1.63-1.57)	50.0-1.90 (1.97-1.90)	50.0-1.85 (1.89-1.85)	50.0-1.86 (1.91-1.86)	50.0-1.57 (1.61-1.57)	49.2-1.85 (1.95-1.85)
R_{merge} (%)	4.2 (15.2)	4.1 (21.4)	9.6 (26.3)	4.3 (17.1)	5.0 (84.5)	3.9 (23.6)	12.0 (87.5)
$I/\sigma I$	41.8 (3.2)	31.8 (5.7)	14.6 (3.5)	30.9 (3.8)	45.1 (2.8)	26.3 (3.3)	15.0 (3.0)
Completeness (%)	91.4 (99.2)	99.8 (99.0)	95.1 (76.8)	92.1 (69.1)	98.3 (96.3)	99.7 (97.6)	100.0 (100.0)
Redundancy	6.6 (4.2)	4.4 (3.9)	4.3 (3.9)	3.8 (2.7)	7.1 (7.1)	4.5 (3.8)	7.1 (6.3)
No. unique reflections	13,040	22,107	11,646	11,884	24,650	28,759	18,676
Refinement							
Resolution (Å)	49.50-1.90	26.40-1.57	40.70-1.90	43.60-1.85	66.50-1.86	46.90-1.57	39.86-1.85
No. reflections	12,360	20,989	11,076	11,304	23,398	27,265	17,701
R_{work} / R_{free}	21.8/25.5	17.4 / 20.5	22.7 / 26.9	18.1 / 21.3	19.4/23.0	16.4 / 19.5	18.7 / 22.2
No. atoms							
Protein	1,207	1,261	1,200	1,264	1804	1,249	1,258
Water	49	139	21	78	137	183	117
Ions	0	3	0	0	17	0	0
Ligand/Peptide	0	130	79	84	68	109	119
Average B-factors (Å^2)							
Protein	25.7	12.2	18.4	26.7	19.3	14.1	19.7
Water	30.2	21.3	19.2	30.6	25.7	22.9	24.5
Ions	N/A	17.1	N/A	N/A	46.0	N/A	N/A
Ligand/Peptide	N/A	15.0	20.6	26.3	37.1	19.5	28.6
R.m.s. deviations							
Bond lengths (Å)	0.022	0.011	0.010	0.011	0.017	0.009	0.017
Bond angles (º)	1.8	1.2	1.1	1.2	1.5	1.2	1.5

*Values in parentheses are for the highest-resolution shell.

References

1. Yang, X., W. H. Lee, F. Sobott, E. Papagrigoriou, C. V. Robinson, J. G. Grossmann, M. Sundstrom, D. A. Doyle, and J. M. Elkins. 2006. Structural basis for protein-protein interactions in the 14-3-3 protein family. *Proc Natl Acad Sci U S A* 103:17237-17242.
2. Otwinowski, Z., and W. Minor. 1997. *Processing of X-ray Diffraction Data Collected in Oscillation Mode*.
3. Kabsch, W. 2010. Xds. *Acta Crystallogr D Biol Crystallogr* 66:125-132.
4. Evans, P. R. 2011. An introduction to data reduction: space-group determination, scaling and intensity statistics. *Acta Crystallogr D Biol Crystallogr* 67:282-292.
5. Evans, P. 2006. Scaling and assessment of data quality. *Acta Crystallogr D Biol Crystallogr* 62:72-82.
6. Vagin, A., and A. Teplyakov. 2010. Molecular replacement with MOLREP. *Acta Crystallogr D Biol Crystallogr* 66:22-25.
7. McCoy, A. J., R. W. Grosse-Kunstleve, P. D. Adams, M. D. Winn, L. C. Storoni, and R. J. Read. 2007. Phaser crystallographic software. *J Appl Crystallogr* 40:658-674.
8. Emsley, P., and K. Cowtan. 2004. Coot: model-building tools for molecular graphics. *Acta Crystallogr D Biol Crystallogr* 60:2126-2132.
9. Murshudov, G. N., A. A. Vagin, and E. J. Dodson. 1997. Refinement of macromolecular structures by the maximum-likelihood method. *Acta Crystallogr D Biol Crystallogr* 53:240-255.
10. Winn, M. D., M. N. Isupov, and G. N. Murshudov. 2001. Use of TLS parameters to model anisotropic displacements in macromolecular refinement. *Acta Crystallogr D Biol Crystallogr* 57:122-133.
11. Chen, V. B., W. B. Arendall, 3rd, J. J. Headd, D. A. Keedy, R. M. Immormino, G. J. Kapral, L. W. Murray, J. S. Richardson, and D. C. Richardson. 2010. MolProbity: all-atom structure validation for macromolecular crystallography. *Acta Crystallogr D Biol Crystallogr* 66:12-21.
12. Schuttelkopf, A. W., and D. M. van Aalten. 2004. PRODRG: a tool for high-throughput crystallography of protein-ligand complexes. *Acta Crystallogr D Biol Crystallogr* 60:1355-1363.
13. Mak, A. N., P. Bradley, R. A. Cernadas, A. J. Bogdanove, and B. L. Stoddard. 2012. The crystal structure of TAL effector PthXo1 bound to its DNA target. *Science* 335:716-719.
14. Deng, D., C. Yan, X. Pan, M. Mahfouz, J. Wang, J. K. Zhu, Y. Shi, and N. Yan. 2012. Structural basis for sequence-specific recognition of DNA by TAL effectors. *Science* 335:720-723.